

# Nonlocal boundary conditions for corrugated acoustic metasurface with strong near-field interactions

Logan Schwan,<sup>1</sup> Olga Umnova,<sup>2</sup> Claude Boutin,<sup>3</sup> and Jean-Philippe Groby<sup>1</sup>

<sup>1</sup>*LAUM, UMR CNRS 6613, Le Mans Université, Avenue Messiaen, Le Mans cedex 09, France<sup>a)</sup>*

<sup>2</sup>*Acoustics Research Centre, University of Salford, Newton Building, Salford M5 4WT, United Kingdom*

<sup>3</sup>*ENTPE/LGCB, UMR CNRS 5513, CeLya, Université de Lyon, Rue Audin, Vaulx-en-Velin, France*

(Dated: 23 December 2017)

The propagation of long-wavelength sound in the presence of a metasurface made by arranging acoustic resonators periodically upon or slightly above an impervious substrate is studied. The method of two-scale asymptotic homogenization is used to derive effective boundary conditions which account for both the surface corrugation and the low-frequency resonance. This method is applied to periodic arrays of resonators of any shape operating in the long-wavelength regime. The approach relies on the existence of the locally periodic boundary layer developed in the vicinity of the metasurface, where strong near-field interactions of the resonators with each other and with the substrate take place. These local effects give rise to an effective surface admittance supplemented by nonlocal contributions from the simple and double gradients of the pressure at the surface. These phenomena are illustrated for the periodic array of cylindrical Helmholtz resonators with an extended inner duct. Effects of the centre-to-centre spacing and orientation of the resonators' opening on the nonlocality and apparent resonance frequency are studied. The model could be used to design metasurfaces with specific effective boundary conditions required for particular applications.

## INTRODUCTION

Structured surfaces made of the two-dimensional (2-D) periodic arrangements of resonators have attracted substantial interest recently as they provide light-weight and low-invasive solutions to control wavefields. When the wavelength around the resonance is significantly longer than the spatial period of the array, these structured surfaces can be referred to as "metasurfaces". The ability of metasurfaces to control wavefields have already been demonstrated in many domains of physics, such as electromagnetism,<sup>1</sup> elastodynamics,<sup>2</sup> and acoustics.<sup>3,4</sup> Meanwhile, the development of equivalent continuum models to describe and characterise metasurfaces has become a central issue from both the theoretical and computational points of view. A common phenomenological approach to the characterisation of a metasurface interior to the unbounded space ("transmit-arrays" or metascreens) is to consider it as an effective layer of subwavelength thickness. Assuming that the behaviour of the effective layer complies with standard continuum theories, such as an effective fluid model in acoustics,<sup>5,6</sup> its presumed effective properties (density and bulk modulus in acoustics) are usually retrieved numerically or experimentally from the fields specularly reflected from and transmitted through the metasurface when it is submitted to a normally incident plane wave.<sup>7</sup> However, the exact physical reasons relating these effective properties

to the surface microstructure can be difficult to identify. Moreover, such procedure can be less straightforward for a "reflect-array", that is a metasurface backed by a substrate impervious to transmission, since only the reflection coefficient is available in that case.

In this work, an analytical approach to the description, characterisation, and design of the acoustic resonant metasurface arranged against an impervious substrate is presented. It relies on the theory of two-scale asymptotic homogenisation<sup>8,9</sup> to determine the macroscopic description of the metasurface, that is the definition of the effective fields, the equations governing them, and the effective constitutive parameters. This is possible if the condition of scale separation  $\epsilon = \ell/L < 1$  is satisfied, where  $\ell$  is the characteristic size of the metasurface unit cell, and  $L$  is the characteristic length of the macroscopic wave. While this method was initially formulated to describe heterogeneous bulk media,<sup>8,9</sup> it has been adapted since to deal with the problem of structured surfaces by means of boundary layer formulations.<sup>10-14</sup> Recently, such a formulation has been applied to the present problem,<sup>4</sup> with a description limited to the leading order of the asymptotic expansions. It was demonstrated that the metasurface can be described by an effective surface admittance of local reaction with parameters explicitly upscaled from the microstructures. In practice, this description is all the more reliable that the scale parameter  $\epsilon$  is considerably less than unity, which has been demonstrated experimentally.<sup>4</sup> However, when the metasurface is corrugated, for instance when resonators are arranged upon the substrate rather than buried in it, the effects of roughness can become noticeable<sup>15</sup> when the wavelength

<sup>a)</sup>Electronic mail: logan.schwan@gmail.com

$L$  is not very large compared to the microstructure size  $\ell$  (but still with  $\epsilon < 1$ ) similar to Rayleigh scattering in 3D media.<sup>16</sup> Also, discrepancies in the value of the resonance frequency have been observed between the theoretical model and the experiments, which become more significant as the scale parameter  $\epsilon$  approaches unity.<sup>4</sup> This effect is attributed to near-field interactions between the resonators in the array which modify the so called "end correction". To account for these effects, the method of two-scale asymptotic homogenisation offers the possibility to improve the leading order description with correctors by considering higher order terms in the asymptotic expansions. This approach, first applied to the description of heterogeneous bulk media,<sup>16–18</sup> has also been used for structured surfaces<sup>10–14,19–22</sup> and leads to nonlocal boundary conditions. Here, the approach is applied to the case of the corrugated resonant metasurface to formulate the effective nonlocal boundary conditions emerging from the combined effects of corrugation and surface resonance. In Section I, the homogenisation model for the metasurface is presented, where the macroscopic description is derived up to the first corrector and nonlocal boundary conditions are formulated. In Section II, the periodic array of slotted cylinders arranged above a rigid substrate is studied as an example. In particular, the influence of the strong near-field interactions of the resonators with each other and with the substrate on the macroscopic properties is illustrated.

## I. BOUNDARY LAYER HOMOGENISATION MODEL

The propagation of airborne low frequency sound in the presence of the corrugated resonant metasurface under ambient conditions is studied, with the atmospheric pressure  $P_0$ , the adiabatic constant  $\gamma$ , the bulk modulus  $B_0 = \gamma P_0$ , the density  $\rho_0$  and the sound speed  $c = \sqrt{B_0/\rho_0}$ . The metasurface consists of the 2-D  $\Sigma$ -periodic arrangement of linear acoustic resonators above the plane surface  $\Gamma_s$  having the unit normal vector  $\mathbf{n}_s$  directed into air, see Figure 1. The impervious substrate  $\Gamma_s$  is not necessarily rigid, but its rheology is supposed to comply with the  $\Sigma$ -periodicity. The resonator above the reference period  $\Sigma$  has the boundary  $\Gamma_r$  with the unit normal vector  $\mathbf{n}_r$  directed into air. For the sake of generality, it is positioned slightly above the surface  $\Gamma_s$ , but the model will allow  $\Gamma_s$  and  $\Gamma_r$  to be connected. The analysis is performed in the linear harmonic regime with the implicit time factor  $e^{-i\omega t}$ . In this system, the pressure  $p$  and particle velocity  $\mathbf{v}$  satisfy the equations of momentum and mass conservation:

$$i\omega\rho_0\mathbf{v} = \mathbf{grad}(p), \quad \text{and} \quad i\omega p = B_0\text{div}(\mathbf{v}), \quad (1)$$

along with Sommerfeld radiation conditions away from the metasurface, and the following boundary conditions at the surface  $\Gamma_r$  and  $\Gamma_s$  of the resonators and substrate:

$$\mathbf{v} \cdot \mathbf{n}_s = \mathcal{R}^s(p) \cdot \mathbf{n}_s \text{ at } \Gamma_s; \quad \mathbf{v} \cdot \mathbf{n}_r = \mathcal{R}^r(p) \cdot \mathbf{n}_r \text{ at } \Gamma_r. \quad (2)$$

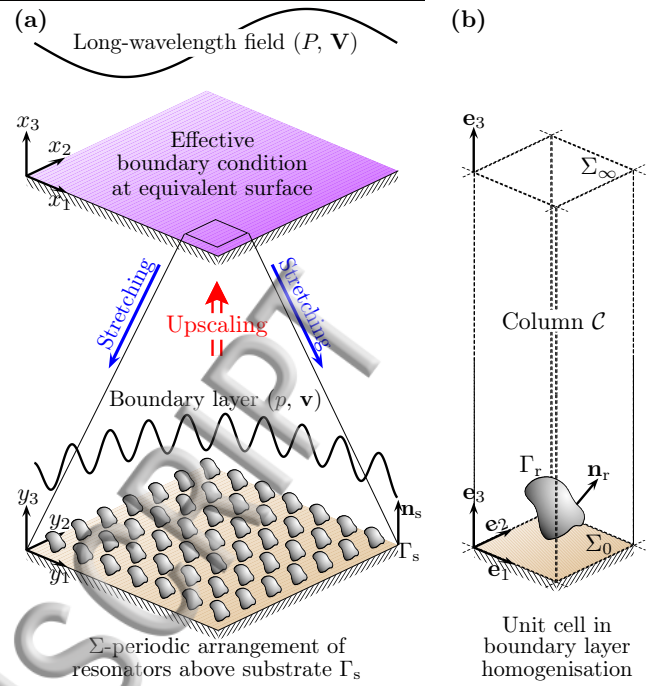


FIG. 1. Illustration of the homogenisation method. (a) Upscaling the boundary layer produced by the array of resonators above the substrate, the metasurface is described in terms of effective boundary conditions for the long-wavelength fields. (b) Unit cell used for homogenisation. (Color online)

In Eq. (2),  $\mathcal{R}^s$  and  $\mathcal{R}^r$  are linear operators describing the velocity distribution prescribed by the substrate and the resonator at the boundaries  $\Gamma_s$  and  $\Gamma_r$  in response to the pressure  $p$  acting on them. The operators  $\mathcal{R}^s$  and  $\mathcal{R}^r$  are generalised response functions which incorporate the phenomena taking place inside the resonators and the substrate. In this sub-structuring approach,  $\mathcal{R}^s$  describes the linear dependence of the velocity  $\mathbf{v}$  at one point  $\mathbf{x}$  of the surface  $\Gamma_s$  on the value of the pressure  $p$  at any other point  $\mathbf{x}'$  of  $\Gamma_s$ , while  $\mathcal{R}^r$  provides such a description for the surface  $\Gamma_r$ . Hence,  $\mathcal{R}^s(p)$  can be written in the form:

$$\mathcal{R}^s(p)(\mathbf{x} \in \Gamma_r) = \int_{\mathbf{x}' \in \Gamma_s} \hat{\mathcal{R}}^s(\mathbf{x}, \mathbf{x}', \omega) p(\mathbf{x}', \omega) d\mathbf{x}', \quad (3)$$

where  $\hat{\mathcal{R}}^s$  is the  $\Sigma$ -periodic kernel of  $\mathcal{R}^s$ . An equation similar to (3) holds for  $\mathcal{R}^r$  with the kernel  $\hat{\mathcal{R}}^r$  and integration over  $\Gamma_r$ . Here, it is assumed that (i) the modelling of the resonators' and substrate's response has been already performed, that is  $\hat{\mathcal{R}}^s$  and  $\hat{\mathcal{R}}^r$  are known; and (ii) the resulting effective conditions given by Eq. (2) can be used in the homogenisation procedure that follows.

### A. Boundary layer homogenisation procedure

The problem stated by Eqs. (1) and (2) is studied for frequencies  $\omega$  close to the resonance frequency  $\omega_o$  of the

resonators, and sufficiently low for the condition of scale separation  $\epsilon = \ell/L < 1$  to be satisfied. Here  $\ell$  is the characteristic size of both the period  $\Sigma$  and the resonators in the direction defined by the vector  $\mathbf{n}_s$ , and  $L = \mathcal{O}(c/\omega)$  is the characteristic length of the macroscopic wavefield. This introduces two scales in the system: the macro-scale  $\mathcal{O}(L)$  related to the Long-Wavelength (LW) field, and the micro-scale  $\mathcal{O}(\ell)$  related to the metasurface array.

When subjected to a LW excitation, the metasurface produces locally  $\Sigma$ -periodic perturbations in the vicinity of the surface  $\Gamma_s$  that vanish some distance away from it. This situation corresponds to a Boundary Layer (BL) problem, which is studied here in the framework of the two-scale asymptotic homogenisation (performed in the tangential directions) coupled with the method of matched asymptotic expansion (in the normal direction), as proposed by Nguentseng & Sanchez-Palencia<sup>10</sup> and used in other studies.<sup>14,21</sup>

Firstly, two space variables are introduced: the usual position vector  $\mathbf{x}$  for the macroscopic description, and the auxiliary vector of stretched coordinates  $\mathbf{y} = \epsilon^{-1}\mathbf{x}$  to describe the surface microstructures. Here, the Cartesian coordinate system  $(O, \mathbf{e}_1, \mathbf{e}_2, \mathbf{e}_3)$  is used, where the origin  $O$  belongs to the substrate  $\Gamma_s$ , the vectors  $(\mathbf{e}_1, \mathbf{e}_2)$  are in the plane  $\Gamma_s$ , and  $\mathbf{e}_3 = \mathbf{e}_1 \wedge \mathbf{e}_2 = \mathbf{n}_s$ , see Figure 1. Using the Einstein convention of implicit summation on repeated indexes, the space variables read  $\mathbf{x} = x_j \mathbf{e}_j$  and  $\mathbf{y} = y_j \mathbf{e}_j$  with  $j \in \{1, 2, 3\}$ . Their tangential components  $\mathbf{x}_S = x_1 \mathbf{e}_1 + x_2 \mathbf{e}_2$  and  $\mathbf{y}_S = y_1 \mathbf{e}_1 + y_2 \mathbf{e}_2$  are also defined.

Secondly, the fields  $p$  and  $\mathbf{v}$  are expanded asymptotically in powers of the scale parameter  $\epsilon$  as follows. Away from the metasurface, the fields  $p$  and  $\mathbf{v}$  experience LW variations only, and their asymptotic expansions involve LW fields  $(P^{(n)}, \mathbf{V}^{(n)})$  that depend only on  $\mathbf{x}$ , where the bracketed superscripts indicate the order of the terms:

$$\begin{cases} p = P^{(0)}(\mathbf{x}) + \epsilon P^{(1)}(\mathbf{x}) + \epsilon^2 \dots, \\ \mathbf{v} = \mathbf{V}^{(0)}(\mathbf{x}) + \epsilon \mathbf{V}^{(1)}(\mathbf{x}) + \epsilon^2 \dots \end{cases} \quad (4)$$

In the vicinity of the surface, however, the problem is somewhat different, due to the presence of the resonators which induce locally  $\Sigma$ -periodic perturbations. According to two-scale asymptotic homogenisation<sup>8,10</sup>, the pressure  $p$  and particle velocity  $\mathbf{v}$  in the boundary layer are set to depend on  $\mathbf{x}_S$ ,  $\mathbf{y}_S$  and  $y_3$  to describe their macroscopic variations in the tangential directions, their local  $\Sigma$ -periodicity close to the surface, and their local fluctuations in the normal direction respectively. Hence, their asymptotic expansions close to the metasurface involve the BL fields  $(p^{(n)}, \mathbf{v}^{(n)})$  as follows:

$$\begin{cases} p = p^{(0)}(\mathbf{x}_S, \mathbf{y}_S, y_3) + \epsilon p^{(1)}(\mathbf{x}_S, \mathbf{y}_S, y_3) + \epsilon^2 \dots, \\ \mathbf{v} = \mathbf{v}^{(0)}(\mathbf{x}_S, \mathbf{y}_S, y_3) + \epsilon \mathbf{v}^{(1)}(\mathbf{x}_S, \mathbf{y}_S, y_3) + \epsilon^2 \dots \end{cases} \quad (5)$$

Since  $(p^{(n)}, \mathbf{v}^{(n)})$  are assumed  $\Sigma$ -periodic over  $\mathbf{y}_S$ , it will be useful to consider the column of air  $\mathcal{C} = \Sigma \times [0, \infty]$  containing the points with  $\mathbf{y}_S$  that belong to the two-dimensional period  $\Sigma$  and  $y_3$  takes the values in  $[0, \infty]$ ,

see Figure 1(b). The cross-sections of  $\mathcal{C}$  located at  $y_3 = 0$  and  $y_3 = \infty$  are denoted  $\Sigma_0$  and  $\Sigma_\infty$  respectively.

Thirdly, the use of the two-scale spatial description modifies the differential operators so that  $\nabla = \nabla_{\mathbf{x}}$  away from the metasurface, and  $\nabla = \nabla_{\mathbf{x}}^S + \epsilon^{-1} \nabla_{\mathbf{y}}$  in the boundary layer region, where  $\nabla_{\mathbf{x}}$ ,  $\nabla_{\mathbf{x}}^S$  and  $\nabla_{\mathbf{y}}$  are the *del* operators with respect to  $\mathbf{x}$ ,  $\mathbf{x}_S$  and  $\mathbf{y}$  respectively. The governing equations (1) and (2) need to be re-written accordingly. Substituting Eq. (4) into (1), and collecting terms of equal powers of  $\epsilon$ , the LW fields  $(P^{(n)}, \mathbf{V}^{(n)})$  are found to satisfy the following equations of momentum and mass conservation:

$$\forall n \geq 0, \quad i\omega \rho_0 \mathbf{V}^{(n)} = \mathbf{grad}_{\mathbf{x}}(P^{(n)}), \quad (6a)$$

$$\forall n \geq 0, \quad i\omega P^{(n)}/B_0 = \text{div}_{\mathbf{x}}(\mathbf{V}^{(n)}). \quad (6b)$$

Similarly, substitution of Eq. (5) into (1) leads to the following equations for the BL fields  $(p^{(n)}, \mathbf{v}^{(n)})$  with  $n \in \{0, 1\}$ :

$$\mathbf{grad}_{\mathbf{y}}(p^{(0)}) = \mathbf{0}, \quad (7a)$$

$$\text{div}_{\mathbf{y}}(\mathbf{v}^{(0)}) = 0, \quad (7b)$$

$$i\omega \rho_0 \mathbf{v}^{(0)} = \mathbf{grad}_{\mathbf{x}}^S(p^{(0)}) + \mathbf{grad}_{\mathbf{y}}(p^{(1)}), \quad (7c)$$

$$i\omega p^{(0)}/B_0 = \text{div}_{\mathbf{x}}^S(\mathbf{v}^{(0)}) + \text{div}_{\mathbf{y}}(\mathbf{v}^{(1)}). \quad (7d)$$

As for the boundary conditions (2), it is important to note that the response functions as defined in Eq. (3) for the substrate and the resonators depend spatially on the variable of micro-description  $\mathbf{y}$  only, since no macroscopic modulation of their rheology is considered here. For this reason, the dependence of the response functions on the space variable  $\mathbf{y}$  is recalled by a subscript as  $\mathcal{R}_{\mathbf{y}}^s$  and  $\mathcal{R}_{\mathbf{y}}^r$ . Further, due to the symmetry in the boundary conditions (2) on  $\Gamma_s$  and  $\Gamma_r$ , the overall boundary  $\Gamma = \Sigma_0 \cup \Gamma_r$  in the column  $\mathcal{C}$  is defined, with the unit normal vector  $\mathbf{n}$  such that  $\mathbf{n} = \mathbf{n}_s$  at  $\Sigma_0$  and  $\mathbf{n} = \mathbf{n}_r$  at  $\Gamma_r$ . The response function  $\mathcal{R}_{\mathbf{y}}$  over  $\Gamma$  is also defined, with  $\mathcal{R}_{\mathbf{y}} = \mathcal{R}_{\mathbf{y}}^s$  at  $\Gamma_s$  and  $\mathcal{R}_{\mathbf{y}} = \mathcal{R}_{\mathbf{y}}^r$  at  $\Gamma_r$ . With those notations, substitution of the asymptotic expansions (5) into (2) yields:

$$\forall n \geq 0, \quad \mathbf{v}^{(n)} \cdot \mathbf{n} = \mathcal{R}_{\mathbf{y}}(p^{(n)}) \cdot \mathbf{n} \text{ at } \Gamma. \quad (8)$$

Finally, asymptotic matching conditions for the LW and BL fields are added according to which the inner limit (as  $x_3 \rightarrow 0$ ) of the LW fields must match the outer limit (as  $y_3 \rightarrow \infty$ ) of the BL fields. The following matching conditions are considered<sup>10,11,19</sup> for the orders  $\epsilon^0$  and  $\epsilon^1$ :

$$\lim_{y_3 \rightarrow \infty} p^{(0)}(\mathbf{x}_S, \mathbf{y}) = P_0^{(0)}(\mathbf{x}_S), \quad (9a)$$

$$\lim_{y_3 \rightarrow \infty} \mathbf{v}^{(0)}(\mathbf{x}_S, \mathbf{y}) = \mathbf{V}_0^{(0)}(\mathbf{x}_S). \quad (9b)$$

$$\lim_{y_3 \rightarrow \infty} [p^{(1)}(\mathbf{x}_S, \mathbf{y}) - y_3 \frac{\partial P^{(0)}}{\partial x_3}(\mathbf{x}_S, 0)] = P_0^{(1)}(\mathbf{x}_S), \quad (9c)$$

$$\lim_{y_3 \rightarrow \infty} [\mathbf{v}^{(1)}(\mathbf{x}_S, \mathbf{y}) - y_3 \frac{\partial \mathbf{V}^{(0)}}{\partial x_3}(\mathbf{x}_S, 0)] = \mathbf{V}_0^{(1)}(\mathbf{x}_S), \quad (9d)$$

where  $P_0^{(n)}(\mathbf{x}_S) = P^{(n)}(\mathbf{x}_S, x_3 = 0)$  and  $\mathbf{V}_0^{(n)}(\mathbf{x}_S) = \mathbf{V}^{(n)}(\mathbf{x}_S, x_3 = 0)$  are the LW pressure and particle velocity at the surface  $\Gamma_s$  at the order  $\epsilon^n$ . The aim of the homogenisation model is now to upscale the boundary conditions (8) in order to provide effective boundary conditions for the LW fields.

## B. Effective description at the leading order

Equation (7a) shows that the BL pressure  $p^{(0)}$  is independent from  $\mathbf{y}$ : it is purely macroscopic and depends only on  $\mathbf{x}_S$ . Using the matching condition (9a), it is found to be equal to the LW pressure  $P_0^{(0)}$  at the surface:

$$p^{(0)}(\mathbf{x}_S, \mathbf{y}) \equiv p^{(0)}(\mathbf{x}_S) \equiv P_0^{(0)}. \quad (10)$$

According to Eq. (7b), the BL flow is locally incompressible at the leading order. Integrating this equation with respect to  $\mathbf{y}$  over the column  $\mathcal{C}$ , using the divergence theorem, the  $\Sigma$ -periodicity of  $\mathbf{v}^{(0)}$ , and the boundary condition (8), the following relation is found, involving the flux  $Q_y^{(0)}$  produced by the substrate and the resonator:

$$Q_y^{(0)} = \int_{\Gamma} \mathcal{R}_y(p^{(0)}) \cdot \mathbf{n} d\Sigma_y = \int_{\Sigma_\infty} \mathbf{v}^{(0)} \cdot \mathbf{e}_3 d\Sigma_y. \quad (11)$$

Combining Eq. (11) with the matching condition (9b), the following equation of mass conservation is derived:

$$\int_{\Sigma_\infty} \mathbf{v}^{(0)} \cdot \mathbf{e}_3 d\Sigma_y = |\Sigma|_y \mathbf{e}_3 \cdot \mathbf{V}_0^{(0)} = Q_y^{(0)}, \quad (12)$$

where  $|\Sigma|_y = \int_{\Sigma_\infty} d\Sigma_y$  is the  $\mathbf{y}$ -integrated surface area of the period  $\Sigma$ . This means that the LW velocity  $\mathbf{V}_0^{(0)}$  balances the overall flux  $Q_y^{(0)}$  produced at the surface, per unit area of the period  $\Sigma$ . Moreover, using Eqs. (10-12), and the linearity of the operator  $\mathcal{R}_y$ , the flux  $Q_y^{(0)}$  is related to the LW pressure  $P_0^{(0)}$  to result in the effective boundary condition for the LW field at the leading order:

$$\mathbf{V}_0^{(0)} \cdot \mathbf{e}_3 = -\Upsilon P_0^{(0)}, \quad (13)$$

where the effective admittance  $\Upsilon$ , of local reaction is:

$$\Upsilon = -\frac{1}{|\Sigma|_y} \int_{\Gamma} \mathcal{R}_y(1) \cdot \mathbf{n} d\Sigma_y. \quad (14)$$

When the scale separation is sharp, the effective boundary condition (13) is sufficiently accurate to describe the metasurface.<sup>4</sup> However, to account for local effects related to the strong near-field interactions between the microstructures, the terms of order  $\epsilon^1$  need to be incorporated, which requires to derive the BL pressure  $p^{(1)}$ .

## C. Evanescent fields and surface flow

The BL pressure  $p^{(1)}$  is looked for in the form:

$$p^{(1)} = P_0^{(1)}(\mathbf{x}_S) + y_3 \frac{\partial P_0^{(0)}}{\partial x_3} \Big|_{(\mathbf{x}_S, 0)} + p^{*(1)}(\mathbf{x}_S, \mathbf{y}) \quad (15)$$

where  $p^{*(1)}$  is an evanescent field such that  $p^{*(1)} \rightarrow 0$  as  $y_3 \rightarrow \infty$  according to the matching condition (9c). The following evanescent velocity field is also defined:

$$\mathbf{v}^{*(0)}(\mathbf{x}_S, \mathbf{y}) = \mathbf{v}^{(0)}(\mathbf{x}_S, \mathbf{y}) - \mathbf{V}_0^{(0)}, \quad (16)$$

such that  $\mathbf{v}^{*(0)} \rightarrow \mathbf{0}$  as  $y_3 \rightarrow \infty$ , according to the matching condition (9b). Combining Eqs. (15) and (16) with the equations (6a) and (7c) of LW and BL momentum conservation, the following equation of momentum conservation is derived for the evanescent fields:

$$i\omega\rho_0\mathbf{v}^{*(0)} = \mathbf{grad}_y(p^{*(1)}). \quad (17)$$

Now, accounting for conditions described by Eqs. (7b), (16), (17), (8), and (13) the problem for the evanescent fields  $p^{*(1)}$  and  $\mathbf{v}^{*(0)}$  takes the form:

$$\text{div}_y(\mathbf{v}^{*(0)}) = 0, \quad (18a)$$

$$i\omega\rho_0\mathbf{v}^{*(0)} = \mathbf{grad}_y(p^{*(1)}), \quad (18b)$$

$$\mathbf{v}^{*(0)} \cdot \mathbf{n} = [\mathcal{R}_y(P_0^{(0)}) - \mathbf{V}_0^{(0)}] \cdot \mathbf{n} \text{ at } \Gamma, \quad (18c)$$

$$\lim_{y_3 \rightarrow \infty} \mathbf{v}^{*(0)} \equiv \mathbf{0} \text{ and } \lim_{y_3 \rightarrow \infty} p^{*(1)} \equiv 0, \quad (18d)$$

$$\mathbf{v}^{*(0)} \text{ and } p^{*(1)} \Sigma\text{-periodic over } \mathbf{y}_S. \quad (18e)$$

Besides, according to the effective boundary condition (13) and the LW momentum conservation (6a), the LW velocity  $\mathbf{V}_0^{(0)}$  at the surface can be written as:

$$\mathbf{V}_0^{(0)} = -\Upsilon P_0^{(0)} \mathbf{e}_3 + \frac{1}{i\omega\rho_0} \mathbf{grad}_x^S(P_0^{(0)}). \quad (19)$$

Now, the weak formulation of the problem (18) is considered with  $\hat{p}$  as a test-field. Multiplying Eq. (18a) by  $\hat{p}/|\Sigma|_y$  and  $\mathbf{y}$ -integrating by parts over the column  $\mathcal{C}$ , while considering the  $\Sigma$ -periodicity and evanescence of the fields, the boundary condition (18c), and Eq. (19), the following relation is found:

$$\mathcal{E}(p^{*(1)}, \hat{p}) = -\frac{i\omega}{c} \mathcal{F}(\hat{p}) P_0^{(0)} - \mathcal{G}(\hat{p}) \cdot \mathbf{grad}_x^S(P_0^{(0)}), \quad (20)$$

where the symmetric definite positive operator  $\mathcal{E}(p^{*(1)}, \hat{p})$  and the linear operators  $\mathcal{F}(\hat{p})$  and  $\mathcal{G}(\hat{p})$  read:

$$\mathcal{E}(p^{*(1)}, \hat{p}) = \frac{1}{|\Sigma|_y} \int_{\mathcal{C}} \mathbf{grad}_y p^{*(1)} \cdot \mathbf{grad}_y \hat{p} d\Omega_y, \quad (21a)$$

$$\mathcal{F}(\hat{p}) = \frac{\rho_0 c}{|\Sigma|_y} \int_{\Gamma} \hat{p} \mathcal{R}_y(1) \cdot \mathbf{n} d\Gamma_y - \rho_0 c \Upsilon \mathcal{G}(\hat{p}) \cdot \mathbf{e}_3, \quad (21b)$$

$$\mathcal{G}(\hat{p}) = -\frac{1}{|\Sigma|_y} \int_{\Gamma} \hat{p} \mathbf{n} d\Gamma_y = \frac{1}{|\Sigma|_y} \int_{\mathcal{C}} \mathbf{grad}_y \hat{p} d\Omega_y. \quad (21c)$$

The divergence theorem, and the  $\Sigma$ -periodicity and evanescence condition for  $\hat{p}$  have been used to derive the second expression of  $\mathcal{G}(\hat{p})$  in Eq. (21c). According to the Lax-Milgram theorem, Eq. (20) entails the existence and uniqueness of the solution for  $p^{*(1)}$ . This equation

shows that the field  $p^{*(1)}$  is forced linearly by the pressure  $P_0^{(0)}$  and the components of its tangential gradient  $\mathbf{grad}_x^S(P_0^{(0)})$ . Hence, it can be written in the form:

$$p^{*(1)}(\mathbf{x}_S, \mathbf{y}) = -\frac{i\omega}{c} d^{*(1)} P_0^{(0)} - \mathbf{b}_S^{*(1)} \cdot \mathbf{grad}_x^S(P_0^{(0)}), \quad (22)$$

where  $d^{*(1)}(\mathbf{y})$  and  $\mathbf{b}_S^{*(1)}(\mathbf{y}) = b_i^{*(1)} \mathbf{e}_i$  with  $i \in \{1, 2\}$  have the dimension of a length, and satisfy the cell problems:

$$\mathcal{E}(d^{*(1)}, \hat{p}) = \mathcal{F}(\hat{p}), \quad \mathcal{E}(b_i^{*(1)}, \hat{p}) = \mathcal{G}(\hat{p}) \cdot \mathbf{e}_i. \quad (23)$$

These cell problems are described in their strong formulation in Appendix A. Interestingly, the one for  $\mathbf{b}_S^{*(1)}$  is similar to that defining the diffusion tensor in the asymptotic homogenisation of periodic porous media<sup>9,23</sup> except that periodicity conditions in the normal direction are replaced here by those of rigid boundary at  $\Sigma_0$  and evanescence at  $\Sigma_\infty$ . While  $\mathbf{b}_S^{*(1)}$  is a purely geometrical and real-valued field, the field  $d^{*(1)}$  can be complex-valued and depends on the frequency  $\omega$  due to the frequency-dependent response function  $\mathcal{R}_y$ . The field  $d^{*(1)}$  is related to the local flux distribution, see Eq. (21b), while  $\mathbf{b}_S^{*(1)}$  is related to the corrugation, since  $\mathcal{G}(\hat{p}) \cdot \mathbf{e}_i = 0$  and hence  $\mathbf{b}_S^{*(1)} \equiv \mathbf{0}$  for a plane surface  $\Gamma$ . Using the symmetry and positiveness of  $\mathcal{E}$ , the following relations result from the cell problems (23) for  $i, j \in \{1, 2\}$ :

$$\mathcal{E}(d^{*(1)}, b_i^{*(1)}) = \mathcal{F}(b_i^{*(1)}) = \mathcal{G}(d^{*(1)}) \cdot \mathbf{e}_i, \quad (24a)$$

$$\mathcal{E}(b_i^{*(1)}, b_j^{*(1)}) = \mathcal{G}(b_j^{*(1)}) \cdot \mathbf{e}_i = \mathcal{G}(b_i^{*(1)}) \cdot \mathbf{e}_j, \quad (24b)$$

$$\mathcal{E}(b_i^{*(1)}, b_i^{*(1)}) = \mathcal{G}(b_i^{*(1)}) \cdot \mathbf{e}_i \geq 0. \quad (24c)$$

Finally, the following vector field is defined, with implicit summation over  $i \in \{1, 2\}$ :

$$\mathbf{W}_S^{(1)}(\mathbf{x}_S) = \frac{1}{|\Sigma|_y} \left( \int_{\mathcal{C}} \mathbf{v}^{*(0)} \cdot \mathbf{e}_i d\Omega_y \right) \mathbf{e}_i. \quad (25)$$

The field  $\mathbf{W}_S^{(1)}(\mathbf{x}_S)$  represents the averaged tangential particle velocity in the vicinity of the surface induced by the evanescent fields. Hence, it will be referred to as *surface flow* in the following. Combining Eq. (25) with (18b), (21c) and (22), the surface flow  $\mathbf{W}_S^{(1)}$  reads:

$$\mathbf{W}_S^{(1)}(\mathbf{x}_S) = -\frac{\mathbf{D}_S^{(1)}}{\rho_0 c} P_0^{(0)} - \frac{\mathbb{B}_S^{(1)}}{i\omega \rho_0} \mathbf{grad}_x^S(P_0^{(0)}), \quad (26)$$

where the tangential vector  $\mathbf{D}_S^{(1)}$  and the  $2 \times 2$  tensor  $\mathbb{B}_S^{(1)}$  have the following components, with  $i, j \in \{1, 2\}$ :

$$\mathbf{D}_S^{(1)}|_i = \mathcal{G}(d^{*(1)}) \cdot \mathbf{e}_i, \quad \mathbb{B}_S^{(1)}|_{ij} = \mathcal{G}(b_j^{*(1)}) \cdot \mathbf{e}_i. \quad (27)$$

Due to the symmetry relations (24b) and (24c), the tensor  $\mathbb{B}_S$  is symmetric definite positive. It is important to note here that the surface flow  $\mathbf{W}_S^{(1)}(\mathbf{x}_S)$  is a purely macroscopic field which is distinct from the LW velocity  $\mathbf{V}_0^{(0)}$ , yet forced by it. It is worth recalling that  $\mathbf{W}_S^{(1)}(\mathbf{x}_S)$  stems from the evanescent fields in the boundary layer induced by the metasurface micro-structures. Note also from Eq. (25) that  $\mathbf{W}_S^{(1)}(\mathbf{x}_S)$  is of the corrector order  $\epsilon^1$ .

#### D. Effective mass conservation at the corrector order $\epsilon^1$

Now that the BL pressure is found, the effective boundary conditions at the corrector order can be derived. First, the particle velocity  $\mathbf{v}^{(1)}$  is looked for in the form:

$$\mathbf{v}^{(1)} = \mathbf{V}_0^{(1)}(\mathbf{x}_S) + y_3 \frac{\partial \mathbf{V}^{(0)}}{\partial x_3} |_{(\mathbf{x}_S, 0)} + \mathbf{v}^{*(1)}(\mathbf{x}_S, \mathbf{y}), \quad (28)$$

where  $\mathbf{v}^{*(1)}$  is an evanescent field such that  $\mathbf{v}^{*(1)} \rightarrow \mathbf{0}$  as  $y_3 \rightarrow \infty$  according to the matching condition (9d). Using Eqs. (16) and (28), the equation (7d) of BL mass conservation is modified as:

$$\operatorname{div}_y(\mathbf{v}^{*(1)}) + \operatorname{div}_x^S(\mathbf{v}^{*(0)}) = 0. \quad (29)$$

Equation (29) is  $\mathbf{y}$ -integrated over the column  $\mathcal{C}$  and the result is divided by  $|\Sigma|_y$ . Using the divergence theorem, the  $\Sigma$ -periodicity and evanescence of  $\mathbf{v}^{*(1)}$ , and the definition (25) of  $\mathbf{W}_S^{(1)}$ , the following relation is derived:

$$\operatorname{div}_x^S(\mathbf{W}_S^{(1)}) = \frac{1}{|\Sigma|_y} \int_{\Gamma} \mathbf{v}^{*(1)} \cdot \mathbf{n} d\Gamma_y. \quad (30)$$

After substitution of Eq. (28) into (30) and application of the boundary condition (8) at the order  $\epsilon^1$ , the equation of mass conservation at the surface is obtained at the order  $\epsilon^1$ :

$$[\mathbf{V}_0^{(1)} \cdot \mathbf{e}_3 + \mathbf{z}^{(1)} \cdot \frac{\partial \mathbf{V}^{(0)}}{\partial x_3}(\mathbf{x}_S, 0)] + \operatorname{div}_x^S(\mathbf{W}_S^{(1)}) = \frac{Q_y^{(1)}}{|\Sigma|_y}, \quad (31)$$

where the corrector order flux  $Q_y^{(1)}$  produced by the substrate and resonator in  $\mathcal{C}$ , and the vector  $\mathbf{z}^{(1)}$  read:

$$Q_y^{(1)} = \int_{\Gamma} \mathcal{R}_y(p^{(1)}) \cdot \mathbf{n} d\Gamma_y, \quad \mathbf{z}^{(1)} = \frac{\int_{\Gamma} y_3 \mathbf{n} d\Gamma_y}{|\Sigma|_y}. \quad (32)$$

Note that  $\mathbf{z}^{(1)}$  has the dimension of a length and has a non-zero component only in the direction  $\mathbf{e}_3$ , that is  $\mathbf{z}^{(1)} = z^{(1)} \mathbf{e}_3$ . Now, combining Eqs. (15), (22) and (32), and using the linearity of  $\mathcal{R}_y$ , the source term  $Q_y^{(1)}/|\Sigma|_y$  in Eq. (31) is found in the form:

$$\frac{Q_y^{(1)}}{|\Sigma|_y} = (\chi^{(1)} + \mu_0^{(1)}) P_0^{(0)} + \frac{\mathbf{A}_S^{(1)}}{\rho_0 c} \cdot \mathbf{grad}_x^S P_0^{(0)} - \Upsilon P_0^{(1)}, \quad (33)$$

where the scalars  $\chi^{(1)}$  and  $\mu_0^{(1)}$  and the components of the vector  $\mathbf{A}_S^{(1)}$  are defined as follows, with  $i \in \{1, 2\}$ :

$$\chi^{(1)} = -\frac{i\omega}{c} \frac{1}{|\Sigma|_y} \int_{\Gamma} \mathcal{R}_y(d^{*(1)}) \cdot \mathbf{n} d\Gamma_y, \quad (34a)$$

$$\mu_0^{(1)} = -\frac{i\omega}{c} \frac{\rho_0 c \Upsilon}{|\Sigma|_y} \int_{\Gamma} \mathcal{R}_y(y_3) \cdot \mathbf{n} d\Gamma_y, \quad (34b)$$

$$\mathbf{A}_S^{(1)}|_i = -\frac{1}{|\Sigma|_y} \int_{\Gamma} \rho_0 c \mathcal{R}_y(b_i^{*(1)}) \cdot \mathbf{n} d\Gamma_y. \quad (34c)$$

The equations (26), (31) and (33) provide the effective description of the metasurface at the corrector order  $\epsilon^1$  and are the main results of this section.

## Discussion on the effective boundary conditions

Before recomposing the asymptotic expansions and re-scaling the fields to the physical space, a discussion should be made here about the nature of the homogenisation model. It results in replacing the corrugated resonant metasurface by an effective boundary condition for the LW field where the exact description of the microstructures is no longer present and surface properties are considered instead. In particular, it means that the surface where the LW fields have to satisfy the effective boundary condition is not corrugated at the local scale but is replaced by an equivalent smooth surface, see Figure 1. That raises the issue of the position of this equivalent surface. It is obvious that it should be located in the vicinity of the metasurface, that is at a height of the order of  $\ell$  above the substrate  $\Gamma_s$ . But positioning it at  $x_3 = 0$  or  $x_3 \sim \ell$  would introduce a phase-shift of the order of  $\epsilon = \ell\omega/c$  in the results. In the approximation of the leading order, the description is valid up to the precision  $\epsilon$ , and such a phase shift is disregarded, as testified by the fact that the pressure is uniform over  $\mathcal{C}$  at the local scale, see Eq. (10). Hence the knowledge of the exact position of the equivalent surface is not required at the leading order, as long as it remains in the vicinity of the metasurface. However, when the homogenisation is performed up to the corrector order, a phase-shift of the order of  $\epsilon$  is no longer within the accuracy of the approximation and the location of the equivalent surface where the effective boundary conditions are applied must be specified. This issue regarding the position of the equivalent surface has already been raised in studies on corrugated substrates<sup>12,14</sup> and is quite similar to the issue of the thickness of the equivalent interface for 2-D arrays of inclusions interior to the unbounded space.<sup>14,20,22</sup>

In the present model, the indication to position the equivalent surface is in fact given by Eq. (31), wherein the first two terms can be seen as the Taylor expansion of the normal component of  $\mathbf{V}$  at the elevation  $z^{(1)}$  above the surface, in the framework of the asymptotic expansions:

$$\mathbf{V}^{(1)}(\mathbf{x}_S, 0) \cdot \mathbf{e}_3 + z^{(1)} \frac{\partial \mathbf{V}^{(0)} \cdot \mathbf{e}_3}{\partial x_3} \Big|_{(\mathbf{x}_S, 0)} = \mathbf{V}^{(1)}(\mathbf{x}_S, \epsilon z^{(1)}) \cdot \mathbf{e}_3. \quad (35)$$

In other words, the equation (31) of mass conservation does not contain the normal component of the velocity calculated at the elevation  $x_3 = 0$  prescribed by the choice of the coordinate system, but, instead, that at the elevation  $x_3 = \epsilon z^{(1)}$ . This position in space represents an averaged height of the corrugation above the substrate and is independent from the choice of the origin of the coordinate system. This quantity is therefore intrinsic to the system, and indicates the position of the equivalent surface. To formulate the boundary conditions at elevation  $x_3 = \epsilon z^{(1)}$ , the LW pressure must be described there. Since  $P^{(0)}$  is uniform at the local scale, see Eq. (10), the pressure  $P_0^{(0)}$  can be replaced in the equations by  $P_z^{(0)} = P^{(0)}(\mathbf{x}_S, \epsilon z^{(1)})$ . However, using

Taylor expansion, the pressure  $P_z^{(1)} = P^{(1)}(\mathbf{x}_S, \epsilon z^{(1)})$  is given by:

$$P_z^{(1)} = P_0^{(1)} + z^{(1)} \frac{\partial P^{(0)}}{\partial x_3} \Big|_{(\mathbf{x}_S, 0)}, \quad (36)$$

which leads to the modification of the coefficient  $\mu_0^{(1)}$  by:

$$\mu^{(1)} = -\frac{i\omega}{c} \frac{\rho_0 c \Upsilon}{|\Sigma|_y} \int_{\Gamma} \mathcal{R}_y(y_3 - z^{(1)}) \cdot \mathbf{n} d\Gamma_y. \quad (37)$$

Now, the leading order and the corrector order solutions for the LW fields are summed together to provide the approximations for the macroscopic pressure and particle velocity, that is  $\mathbf{V} = \mathbf{V}^{(0)} + \epsilon \mathbf{V}^{(1)}$  and  $P = P^{(0)} + \epsilon P^{(1)}$ . The effective parameters identified in the homogenisation scheme are also rescaled to the physical space, with for instance  $z = \epsilon z^{(1)}$  or  $\mu = \epsilon \mu^{(1)}$ . This provides the following effective boundary conditions for the LW fields at the metasurface, where  $\mathcal{S} = Q/|\Sigma|$ :

$$\mathbf{V} \cdot \mathbf{e}_3 + \text{div}_{\mathbf{x}}^S(\mathbf{W}_S) = \mathcal{S} \quad \text{at } x_3 = z, \quad (38a)$$

$$\mathbf{W}_S(\mathbf{x}_S) = -\frac{\mathbf{D}_S}{\rho_0 c} P|_z - \frac{\mathbb{B}_S}{i\omega\rho_0} \mathbf{grad}_{\mathbf{x}}^S(P)|_z, \quad (38b)$$

$$\mathcal{S} = -(\Upsilon - \chi - \mu)P|_z + \frac{\mathbf{A}_S}{\rho_0 c} \cdot \mathbf{grad}_{\mathbf{x}}^S(P)|_z. \quad (38c)$$

Equation (38a) states the effective mass conservation where the source term  $\mathcal{S}$  is related to the flux radiated from the resonators and substrate, and is balanced by two macroscopic fields: the normal component of the LW velocity  $\mathbf{V}$ , and the divergence of the surface flow  $\mathbf{W}_S$ . Equation (38b) provides the rheological relation for the surface flow  $\mathbf{W}_S$ , where the last term, due to the tangential flow of air through the surface corrugation, can be seen as the surface variant of the Darcy Law.<sup>9</sup> Equation (38c) provides the expression for the source term  $\mathcal{S}$ , forced by the LW surface pressure and its tangential gradient. The three equations (38a) to (38c) can be combined to provide the effective surface condition in the form of a single equation:

$$\begin{aligned} \mathbf{V} \cdot \mathbf{e}_3 = & -(\Upsilon - \chi - \mu)P + \frac{\mathbf{A}_S + \mathbf{D}_S}{\rho_0 c} \cdot \mathbf{grad}_{\mathbf{x}}^S(P) \\ & + \frac{\mathbb{B}_S}{i\omega\rho_0} : \mathbf{grad}_{\mathbf{x}}^S[\mathbf{grad}_{\mathbf{x}}^S(P)] \quad \text{at } x_3 = z, \end{aligned} \quad (39)$$

where  $:$  is the tensor double contraction. Equation (39) shows that the normal component of the velocity depends on the simple and second gradients of the pressure at the surface. Hence, microstructural effects result in an effective *nonlocal* boundary conditions for the metasurface. Note that other nonlocal effects induced by microstructures have been reported for elastodynamic metasurfaces<sup>13</sup> and for bulk media,<sup>24–26</sup> despite differences in the physical approaches to describe them. The boundary condition described by Eq. (39) is the final result of the homogenisation model.

## II. APPLICATION

### A. Motivation and description of the metasurface

The aim of this section is to describe the effects of the boundary condition (39) on the sound reflection from the metasurface, and investigate the possibility to achieve the total absorption of sound at the resonance frequency. For this, the metasurface consisting of the array of cylindrical Helmholtz resonators arranged periodically in the direction  $\mathbf{e}_1$  with the period size  $\ell = 42$  mm, and positioned at the distance  $h = 0.02\ell \approx 0.8$  mm above a rigid substrate is studied, see Figure 2(a). The resonators are supposed to be infinitely long with their axes in the direction  $\mathbf{e}_2$ . In the plane  $(\mathbf{e}_1, \mathbf{e}_3)$ , they have the outer diameter  $2r = 29$  mm and the opening  $\Gamma_a$  of width  $e = 1.5$  mm oriented in the direction defined by the angle  $\alpha$  counted from  $\mathbf{e}_1$ . Each resonator consists of a cylindrical inner cavity of diameter  $2r' = 13.4$  mm connected to the outside via a duct of width  $e$  rolled around the inner cavity, see Figure 2(b). The relative positions of the inner and outer apertures is defined by the angle  $\beta = 227^\circ$ . The arc portion of the duct is positioned at equal distance from the boundary of the cavity and the outer boundary  $\Gamma_r$  of the resonator. The inner walls of the resonators are assumed rigid. Plane wave reflection from the metasurface is studied, with  $(\mathbf{e}_1, \mathbf{e}_3)$  as the plane of incidence. Hence, the problem can be solved in the two dimensional Cartesian coordinate system  $(\mathbf{e}_1, \mathbf{e}_3)$ . The reasons leading to the design are explained in Section II C.

### B. Model for the resonators and substrate

Since the substrate is rigid, the following relation holds:  $\mathcal{R}_y^s(p) \cdot \mathbf{n}_s \equiv 0$ . As for the Helmholtz resonator, its boundary  $\Gamma_r$  is rigid, except for the opening  $\Gamma_a$ , which is supposed sufficiently small to make the following assumptions<sup>27</sup>: (i) the radial particle velocity is uniform over the opening  $\Gamma_a$ , with the value  $v_o$ ; and (ii) the velocity  $v_o$  is related to the mean value  $\langle p \rangle = |\Gamma_a|^{-1} \int_{\Gamma_a} p d\Gamma$  of the pressure  $p$  acting at the opening  $\Gamma_a$  by  $v_o = Y \langle p \rangle$ , where  $Y$  is an admittance. Hence, the response function of the overall surface  $\Gamma$  satisfies:

$$\mathcal{R}_y(p) \cdot \mathbf{n} = Y \langle p \rangle \Pi(\mathbf{y}) \quad \text{at } \Gamma, \quad (40)$$

where  $\Pi(\mathbf{y})$  is equal to 1 over  $\Gamma_a$  and 0 elsewhere on  $\Gamma$ . Here, the admittance  $Y$  is computed numerically using the Finite Element Method (FEM) by solving for the pressure  $p_r$  developing inside the resonator in response to unit pressure  $P_a \equiv 1$  applied at the duct outside aperture  $\Gamma_a$ , see inset in Figure 2(c). To do so, the Helmholtz equation,  $\text{div}(\mathbf{grad} p_r) + \omega^2(\rho_r/B_r)p_r = 0$ , is solved, where  $\rho_r$  and  $B_r$  are the effective density and bulk modulus of air in the resonator. In the inner cavity, viscous and thermal losses are neglected<sup>4</sup> and  $\rho_r = \rho_0$  and  $B_r = B_0$  there. In the narrow duct, however, viscous and thermal

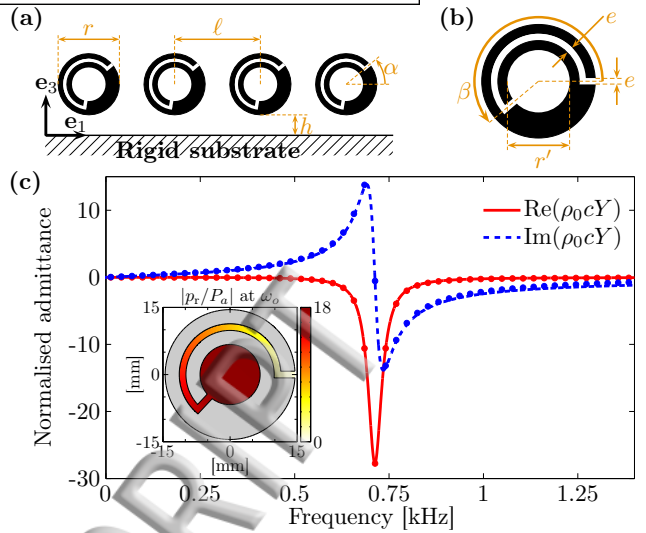


FIG. 2. (a) Periodic arrangement of cylindrical resonators above the rigid substrate. (b) Geometry of a cylindrical Helmholtz resonator with an extended inner duct. (c) Normalised admittance at the duct outside aperture of the Helmholtz resonator considered in the study; the dots are FEM computation points and the lines correspond to the Lorentzian form Eq. (42) with parameters obtained by fitting FEM results. In figure (c), the colour-map represents FEM results for the pressure amplitude inside the resonator in response to a unit pressure  $P_a \equiv 1$  at the duct outside aperture at the resonance. (Color online)

effects are significant, and the effective density and bulk modulus of air in the duct are given by<sup>5,6</sup>:

$$\rho_r = \frac{\rho_0}{1 - \Phi(e/\delta_v)}, \quad B_r = \frac{B_0}{1 + (\gamma - 1)\Phi(e/\delta_t)}, \quad (41)$$

where  $\delta_v = \sqrt{4\nu/(\rho_0\omega)}$  and  $\delta_t = \delta_v/\sqrt{\text{Pr}}$  are viscous and thermal skin-depths, with  $\nu$  and  $\text{Pr}$  being the viscosity and the Prandtl number of air, and where  $\Phi(X) = \tanh(X\sqrt{-i})/(X\sqrt{-i})$  is a form function.<sup>5,6</sup> In this FEM simulation, the admittance  $Y$  is given by  $Y = \langle \mathbf{grad}(p_r) \cdot \mathbf{n}_r \rangle / (i\omega\rho_r)$ , and results are shown in Figure 3(c). The following Lorentzian form is assumed for it:

$$\rho_0 c Y = i\sigma\omega / [\omega_o^2 - i2\xi\omega - \omega^2], \quad (42)$$

where the resonance frequency  $\omega_o$ , the loss factor  $\xi/\omega_o \ll 1$  and the parameter  $\sigma$  are retrieved by fitting Eq. (42) with the FEM results, see Figure 2(c). That provides  $\omega_o/(2\pi) \approx 712.5$  Hz  $\xi/\omega_o \approx 3.1\%$  and  $\sigma/\omega_o \approx 1.71$ .

### C. Effective parameters from the homogenisation model

Now, the effective parameters involved in the boundary conditions (39) can be computed. As the problem considered is two-dimensional, only 7 scalar parameters are required: the admittance coefficients  $\Upsilon$ ,  $\chi$ , and  $\mu$ , the

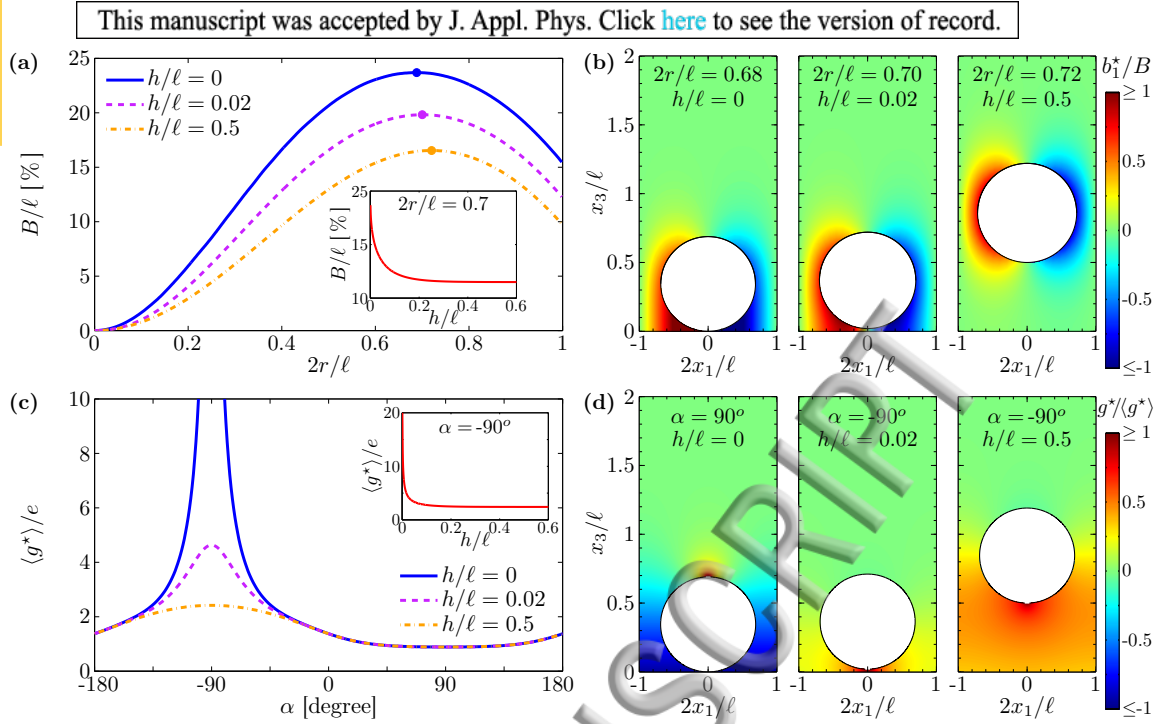


FIG. 3. Numerical solutions for the evanescent fields  $b_1^*$  and  $g^* = d^*/(\rho_0 c Y)$  defined by Eqs. (A1-A2), and analysis of the effective parameters  $B$  and  $\langle g^* \rangle$ . (a) Dependence of  $B$  on the resonator normalised diameter  $2r/\ell$  and elevation  $h/\ell$  above the substrate. (b) Colour-maps of  $b_1^*$  for different values of  $2r/\ell$  and  $h/\ell$ . (c) Dependence of  $\langle g^* \rangle$  on the normalised elevation  $h/\ell$  and orientation angle  $\alpha$  of the resonator opening. (d) Colour-maps of  $g^*$  for different values of  $\alpha$  and  $h/\ell$ . (Color online)

$\mathbf{e}_1$ -components  $A_1 = \mathbf{A}_S \cdot \mathbf{e}_1$  and  $D_1 = \mathbf{D}_S \cdot \mathbf{e}_1$  of the vectors  $\mathbf{A}_S$  and  $\mathbf{D}_S$ , the component  $B = (\mathbb{B}_S \cdot \mathbf{e}_1) \cdot \mathbf{e}_1$  of the tensor  $\mathbb{B}_S$ , and the elevation  $z$  for the equivalent surface. Their expressions can be found in Eqs. (14), (34a), (37), (34c), (27) and (32). Using the response function given by Eq. (40), with the normalised admittance given by Eq. (42), and the symmetry relation given by Eq. (24a), these coefficients are derived in the form:

$$\rho_0 c \Upsilon = -i\eta\omega/[\omega_o^2 - i2\xi\omega - \omega^2], \quad \text{with } \eta = e\sigma/\ell, \quad (43a)$$

$$\chi = i\omega\Upsilon(\rho_0 c Y)\langle g^* \rangle/c, \quad \text{with } g^* = d^*/(\rho_0 c Y), \quad (43b)$$

$$\mu = i\omega\Upsilon(\rho_0 c \Upsilon)\zeta/c, \quad \text{with } \zeta = \langle x_3 - z \rangle, \quad (43c)$$

$$A_1 = \rho_0 c \Upsilon \langle b_1^* \rangle = -D_1, \quad (43d)$$

$$B = \mathcal{G}(b_1^*) \cdot \mathbf{e}_1, \quad \text{and } z = \pi r^2/\ell, \quad (43e)$$

In Eq. (43b), the field  $g^*$  is purely geometrical and real-valued, since it satisfies the same equations (A2) as  $d^*$  except for the boundary condition (A2b) which becomes  $\text{grad}_{\mathbf{y}}(g^{*(1)}) \cdot \mathbf{n} = (2e/\ell)\mathbf{e}_3 \cdot \mathbf{n} - \Pi(\mathbf{y})$  at  $\Gamma$ . In Eq. (43c), the length  $\zeta$  corresponds to the mean distance between the equivalent surface positioned at  $x_3 = z$  and the points of the aperture  $\Gamma_a$ . It can be approximated by  $\zeta \approx h + r(1 + \sin \alpha) - z$  using the relation  $\sin(e/r) \approx e/r$ , where  $e/r \ll 1$  is the angular opening of the aperture  $\Gamma_a$ . In Eq. (43d), the relation  $A_1 = -D_1$  implies that the simple gradient term in the effective boundary condition (39) is not present in the case studied here. This is due to the fact that the plane  $(\mathbf{e}_2, \mathbf{e}_3)$  is a plane of symmetry for the cell  $\mathcal{C}$  when the whole boundary of the

Helmholtz resonator is supposed to be rigid: it leads to the relation  $\mathcal{G}(b_1^*) \cdot \mathbf{e}_3 = 0$  used in the computation of  $D_1$ . In Eq. (43e), the coefficient  $B$  has the dimension of a length. Its expression is related to the field  $b_1^*$  satisfying the cell problem described in Eq. (A1) which depends only on the corrugation. The length  $B$  appears in the effective boundary condition (39), where it weights the term with the double gradient of the pressure. Hence, the length  $B$  characterises, at the macroscopic scale, the micro-corrugation of the surface, and it will be referred to as the *characteristic corrugation length* in what follows. It is worth mentioning also that the position  $z$  of the equivalent surface given by Eq. (43e) is independent from the elevation  $h$  of the resonators above the rigid substrate. Finally, since  $\chi + \mu = \mathcal{O}(\epsilon Y)$ , Taylor expansion is performed to provide:

$$\rho_0 c (\Upsilon - \chi - \mu) \approx \rho_0 c \Upsilon / [1 + i\omega\rho_0 c (Y\langle g^* \rangle + \Upsilon\zeta)/c]. \quad (44)$$

Using the expressions (42) and (43a) for  $\rho_0 c Y$  and  $\rho_0 c \Upsilon$ , the equation (44) is transformed as:

$$\rho_0 c (\Upsilon - \chi - \mu) \approx -i\eta\omega/[\omega_o^2 - i2\xi\omega - (\kappa\omega)^2], \quad (45a)$$

$$\text{where } \kappa = \sqrt{1 + (\langle g^* \rangle/e - \zeta/\ell)e\sigma/c}. \quad (45b)$$

Comparison of Eq. (45) with (43a) shows that the corrector  $\chi + \mu$  changes the apparent resonance frequency from  $\omega_o$  to  $\omega_o/\kappa$ . The resonance frequency of the *single* Helmholtz resonator above the rigid substrate is already known to decrease as the opening of the resonator is oriented towards the substrate.<sup>27</sup> Here, the variations in the

resonance frequency are due to the strong near-field interactions of all the resonators with each other and with the substrate. It is important to note that the value of  $\rho_0 c(\Upsilon - \chi - \mu)$  at the frequency  $\omega_o/\kappa$  is equal to the same value  $\eta/(2\xi)$  as that of the leading order admittance  $\rho_0 c\Upsilon$  at the eigenfrequency  $\omega_o$ . If, according to the leading order calculations, the admittance matching with air,  $\rho_0 c\Upsilon = 1$ , is achieved at the resonance frequency  $\omega_o$ , accounting for the correctors of order  $\epsilon^1$  preserves this condition, but it happens at the frequency  $\omega_o/\kappa$ .

The field  $b_1^*$  is computed numerically solving the cell problem (A1) by means of the FEM. To justify the design, the calculations are performed for different cylinder radius  $r$  and elevation  $h$ . That results in the characteristic corrugation length  $B$  shown in Figure 3(a). For a given elevation  $h$ , the dependence of  $B$  on the normalised radius  $r/\ell$  is not monotonous: its maximum value  $B/\ell \in [0.16, 0.24]$  is reached for  $2r/\ell \in [0.69, 0.72]$ . The characteristic corrugation length  $B$  is larger for cylinders upon the substrate, decreases sharply as the elevation  $h$  increases, see the inset in Figure 3(a), and reaches a stationary value for  $h/\ell \geq 0.3$  approximately. Colour-maps of the field  $b_1^*$  are given in Figures 3(b) for different elevations  $h/\ell$  and at values of  $r/\ell$  for which  $B/\ell$  is maximum. They confirm the fact that  $b_1^*$  is confined to the surface, consistently with the notion of evanescent fields. While a strong interaction between the array and the substrate occurs for cylinders close to the surface  $h \rightarrow 0$ , the field  $b_1^*$  tends to remain confined in the vicinity of the array and nearly vanishes at the substrate when the cylinders are positioned further from it. In this case, the interaction of the array with the substrate is very weak, which explains why  $B/\ell$  reaches its stationary value.

The resonator diameter has been chosen to provide  $2r/\ell \approx 0.69$ , so that  $B/\ell$  is close to its maximum values (which still depend on the elevation  $h$ ) to enhance the effects from the nonlocal contributions. Besides, the duct and cavity of the resonator have been designed according to the following constraints: (i) the scale parameter  $\epsilon_o = \ell\omega_o/c$  at the resonance is equal to  $0.55 < 1$  which is sufficiently close to unity for the corrector term to have noticeable contribution, yet  $\epsilon_o^2 = 0.3$  so that terms of the second corrector order remain small; and (ii) the admittance matching  $\rho_0 c\Upsilon = \eta/(2\xi) = 1$  at the resonance frequency  $\omega_o$  is achieved. Then, the cell problem for the field  $g^*$  is solved numerically using the FEM. Its normalised mean value  $\langle g^* \rangle/e$  over the duct outside aperture is computed for different elevations  $h$  and orientation angles  $\alpha$  of the opening, see Figure 3(c). It shows that, the elevation  $h$  has nearly no effect on  $\langle g^* \rangle$  when the aperture is turned away from the surface:  $\langle g^* \rangle/e$  reached its minimum value  $\approx 0.89$  for the orientation angle  $\alpha = 90^\circ$ , and varies only slightly over the range  $\alpha \in [0, 180^\circ]$  to reach  $\approx 1.4$  at  $\alpha = 0$  and  $\alpha = 180^\circ$ . Conversely, the variations of  $\langle g^* \rangle/e$  with the elevation  $h$  are very significant for  $\alpha \in [-180^\circ, 0]$ , especially when the aperture is facing the rigid substrate at  $\alpha = -90^\circ$ . For that orien-

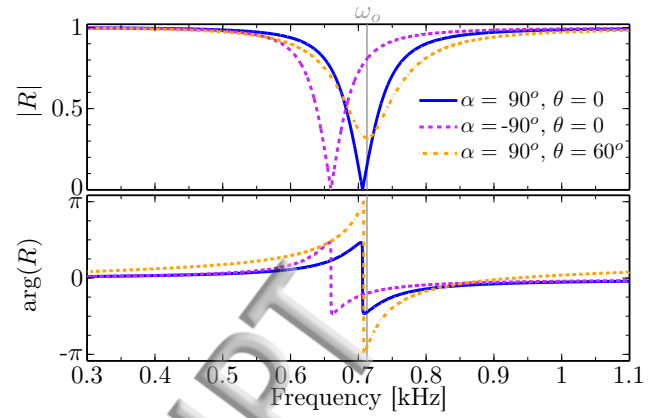


FIG. 4. (a) Amplitude and (b) phase of the reflection coefficient  $R$  for different angles of incidence  $\theta$  and orientation angles  $\alpha$  of the resonators opening. Computations with the elevation  $h/\ell = 0.02$ . (Color online)

tation angle,  $\langle g^* \rangle/e$  reaches its maximum value: it tends to infinity as  $h \rightarrow 0$ , when radiation from the aperture is nearly impossible, and decreases sharply as the elevation  $h$  increases, see inset in Figure 3(c), to reach the stationary value  $\langle g^* \rangle/e \approx 2.4$  for the elevations  $h/\ell \geq 0.3$  approximately. The colour-maps of the field  $g^*$  for different orientation angles  $\alpha$  and elevations  $h$  are provided in Figure 3(d). They confirm that the evanescent field  $g^*$  remains confined to the surface. In addition, it tends to remain mostly located between the inclusions and the rigid backing for  $\alpha \in [-180^\circ, 0]$ .

#### D. Reflection from the metasurface

Finally, the reflection of the incident plane wave  $e^{i\omega(x_1 \sin \theta - (x_3 - z) \cos \theta)/c}$  from the metasurface is studied, where  $\theta$  is the angle of incidence counted from  $\mathbf{e}_3$ . The specularly reflected wave is  $R e^{i\omega(x_1 \sin \theta + (x_3 - z) \cos \theta)/c}$ , where  $R$  is the pressure reflection coefficient. Using Eqs. (39) and (43), the reflection coefficient reads:

$$R = \frac{\cos \theta - \Lambda}{\cos \theta + \Lambda}, \quad \Lambda = \rho_0 c(\Upsilon - \mu - \chi) - \frac{i\omega B \sin^2 \theta}{c}. \quad (46)$$

At normal incidence,  $\theta = 0$ , the nonlocal contribution to the boundary conditions vanish and  $R$  tends to its usual expression for the surface with the admittance  $\Upsilon - \chi - \mu$ . The perfect absorption  $R = 0$  is achieved if  $\theta = 0$  and the critical coupling condition  $\rho_0 c(\Upsilon - \chi - \mu) = 1$  is satisfied. Nonlocal contribution to the boundary conditions becomes significant at oblique and grazing incidence. If the resonators are replaced by rigid scatterers, then  $\Lambda = -i\omega B \sin^2(\theta)/c$ , and the perfect reflection of the wave  $|R| = 1$  is achieved for any angle  $\theta$  and frequency  $\omega$ . The perfect reflection  $|R| = 1$  is also achieved for any angle and frequency for lossless resonators ( $\xi = 0$ ). Nevertheless, a phase shift that depends on  $\theta$  and  $\omega$  is induced in those two cases. The amplitude and phase

of  $P$  are plotted in Figure 4 for  $\theta \in \{0^\circ, 60^\circ\}$  and for the opening orientation angles  $\alpha = \pm 90^\circ$ . The elevation  $y_3/c$  of 0.02 has been chosen. As expected from the design, the perfect absorption of sound  $R = 0$  is achieved at apparent resonance frequencies lower than  $\omega_o$  (by 53 Hz for  $\alpha = -90^\circ$ ) at normal incidence  $\theta = 0$ . At the oblique incidence  $\theta = 60^\circ$ , the sound absorption is lower at the apparent frequency, and an additional phase shift due to the nonlocal contribution can be observed in the reflection coefficient, even at frequencies away from the resonance.

## CONCLUSION

The present study showed that models of local reaction for metasurfaces are valid when a sharp scale separation exists between the sound wavelength and the characteristic size of the surface lattice. However, when the scale separation is not sharp, nonlocal contributions to the effective boundary conditions for the corrugated resonant metasurfaces should be accounted for. The nonlocal effective boundary conditions have been derived accounting for the correctors in the two-scale asymptotic homogenisation analysis. The model developed here has been illustrated for the 2-D array of cylindrical Helmholtz resonators with an extended duct, but the analytical results summarised in Eqs. (38) are valid for 3-D geometry, for any resonators and substrate the behaviour of which can be described by the linear response functions given by Eq. (3), and any LW field satisfying the condition of scale separation. In particular, the non-local contributions should lead to anisotropic effects in 3-D, since the effective nonlocal parameters are tensors. The results are useful for the design of corrugated resonant metasurfaces, where the corrugation/radiation coupling could be used to tune the resonance frequency and the type of boundary conditions by simply changing the orientation of the resonators. Obtaining effective boundary conditions for metasurfaces with more complicated geometry of the elementary cell (when it contains several mistuned resonators for instance) will be the next step in the work.

## ACKNOWLEDGMENTS

The authors gratefully acknowledge S. Taherzadeh and K. Attenborough for their support. L. S. and J.-P. G. are grateful to *RFI Le Mans Acoustique* (Région Pays de la Loire). This work is part of PEALS project funded by the U.K. Engineering and Physical Sciences Research Council under grant agreement EP/K037234/1. The collaboration resulted in this work was also supported by COST (European Cooperation in Science and Technology) Action DENORMS CA15125.

## Appendix A: Cell problems in their strong formulation

The strong formulation of the cell problems (23) reads:

$$\operatorname{div}_{\mathbf{y}}(\mathbf{grad}_{\mathbf{y}}(b_i^{*(1)}) - \mathbf{e}_i) = 0, \quad (\text{A1a})$$

$$(\mathbf{grad}_{\mathbf{y}}(b_i^{*(1)}) - \mathbf{e}_i) \cdot \mathbf{n} = 0 \text{ at } \Gamma, \quad (\text{A1b})$$

$$\lim_{y_3 \rightarrow \infty} \mathbf{grad}_{\mathbf{y}}(b_i^{*(1)}) \equiv \mathbf{0}, \quad (\text{A1c})$$

$$\lim_{y_3 \rightarrow \infty} b_i^{*(1)} \equiv 0 \text{ and } b_i^{*(1)} \Sigma\text{-periodic over } \mathbf{y}_S. \quad (\text{A1d})$$

$$\operatorname{div}_{\mathbf{y}}(\mathbf{grad}_{\mathbf{y}}(d^{*(1)})) = 0, \quad (\text{A2a})$$

$$\mathbf{grad}_{\mathbf{y}}(d^{*(1)}) \cdot \mathbf{n} = -\rho_0 c [\mathcal{R}_{\mathbf{y}}(1) + \Upsilon \mathbf{e}_3] \cdot \mathbf{n} \text{ at } \Gamma, \quad (\text{A2b})$$

$$\lim_{y_3 \rightarrow \infty} \mathbf{grad}_{\mathbf{y}}(d^{*(1)}) \equiv \mathbf{0}, \quad (\text{A2c})$$

$$\lim_{y_3 \rightarrow \infty} d^{*(1)} \equiv 0 \text{ and } d^{*(1)} \Sigma\text{-periodic over } \mathbf{y}_S, \quad (\text{A2d})$$

<sup>1</sup>D. R. Chowdhury, N. Xu, W. Zhang, and R. Singh, J. Appl. Phys. **118**, 023104 (2015).

<sup>2</sup>C. Boutin, L. Schwan, and M. S. Dietz, J. Appl. Phys. **117**, 064902 (2015).

<sup>3</sup>N. Jiménez, W. Huang, V. Romero-García, V. Pagneux, and J.-P. Groby, Appl. Phys. Lett. **109**, 121902 (2016).

<sup>4</sup>L. Schwan, O. Umnova, and C. Boutin, Wave Motion **72**, 154 (2017).

<sup>5</sup>C. Zwikker and C. W. Kosten, *Sound absorbing materials* (Elsevier Publishing Company, 1949).

<sup>6</sup>J.-F. Allard and N. Atalla, *Propagation of Sound in Porous Media* (John Wiley & Sons, Ltd, 2009).

<sup>7</sup>D. R. Smith, S. Schultz, P. Markos, and C. M. Soukoulis, Phys. Rev. B **65**, 195104 (2002).

<sup>8</sup>E. Sanchez-Palencia, *Non-Homogeneous Media and Vibration Theory*, Lecture Notes in Physics, Vol. 127 (Springer-Verlag, Berlin, Heidelberg, 1980).

<sup>9</sup>J.-L. Auriault, C. Boutin, and C. Geindreau, *Homogenization of Coupled Phenomena in Heterogenous Media* (ISTE Ltd and Wiley, 2009).

<sup>10</sup>G. Nguetseng and E. Sanchez-Palencia, "Local effects in the analysis of structures," (Elsevier Science Publishers B. V, 1985) Chap. Stress concentration for defects distributed near a surface, pp. 55–74.

<sup>11</sup>G. Nguetseng, Model. Math. Analyse Num. **19**, 33 (1985).

<sup>12</sup>C. L. Holloway and E. F. Kuester, Radio Sci. **35**, 661 (2000).

<sup>13</sup>C. Boutin and P. Roussillon, Int. J. Eng. Sci. **44**, 180 (2006).

<sup>14</sup>J.-J. Marigo and A. Maurel, J. Acoust. Soc. Am. **140**, 260 (2016).

<sup>15</sup>I. Bashir, S. Taherzadeh, and K. Attenborough, J. Acoust. Soc. Am. **133**, 1281 (2013).

<sup>16</sup>C. Boutin, J. Acoust. Soc. Am. **122**, 1888 (2007).

<sup>17</sup>C. Boutin, Int. J. Heat Mass Transfer **38**, 3181 (1995).

<sup>18</sup>C. Boutin, Int. J. Solids Structures **33**, 1023 (1996).

<sup>19</sup>J.-J. Marigo and C. Pideri, Int. J. Damage Mech. **20**, 1151 (2011).

<sup>20</sup>B. Delourme, H. Haddar, and P. Joly, J. Math. Pures Appl. **98**, 28 (2012).

<sup>21</sup>J.-J. Marigo and A. Maurel, Proc. R. Soc. A **472**, 20160068 (2016).

<sup>22</sup>J.-J. Marigo, A. Maurel, K. Pham, and A. Sbitti, J. Elasticity **128**, 265 (2017).

<sup>23</sup>J.-L. Auriault and J. Lewandowska, Geotechnique **43**, 457 (1993).

<sup>24</sup>P. Germain, SIAM J. Appl. Mathematics **25**, 556 (1973).

<sup>25</sup>J. Soubestre and C. Boutin, Mech. Mater. **55**, 16 (2012).

<sup>26</sup>D. Lafarge and N. Nemati, Wave Motion **50**, 1016 (2013).

<sup>27</sup>C. Lagarrigue, J.-P. Groby, V. Tournat, O. Dazel, and O. Umnova, J. Acoust. Soc. Am. **134**, 4670 (2013).

